J. Non-Newtonian Fluid Mech. 165 (2010) 901–913

Contents lists available at ScienceDirect

Journal of Non-Newtonian Fluid Mechanics

journal homepage: www.elsevier.com/locate/jnnfm

Laminar natural convection of Bingham fluids in a square enclosure with differentially heated side walls

Osman Turan [a,b], Nilanjan Chakraborty [a], Robert J. Poole [a,*]

[a] Department of Engineering, University of Liverpool, Brownlow Hill, Liverpool L69 3GH, UK
[b] Department of Mechanical Engineering, Karadeniz Technical University, Trabzon 61080, Turkey

ARTICLE INFO

Article history:
Received 9 March 2010
Received in revised form 23 April 2010
Accepted 26 April 2010

Keywords:
Natural convection
Yield stress
Bingham model
Heat transfer

ABSTRACT

In this study, two-dimensional steady-state simulations of laminar natural convection in square enclosures with differentially heated sidewalls have been carried out where the enclosures are considered to be completely filled with a yield stress fluid obeying the Bingham model. Yield stress effects on heat and momentum transport are investigated for nominal values of Rayleigh number (Ra) in the range 10^3–10^6 and a Prandtl number (Pr) range of 0.1–100. It is found that the mean Nusselt number $\overline{Nu}$ increases with increasing values of Rayleigh number for both Newtonian and Bingham fluids. However, $\overline{Nu}$ values obtained for Bingham fluids are smaller than that obtained in the case of Newtonian fluids with the same nominal value of Rayleigh number Ra due to weakening of convective transport. The mean Nusselt number $\overline{Nu}$ in the case of Bingham fluids is found to decrease with increasing Bingham number, and, for large values of Bingham number Bn, the value settles to unity ($\overline{Nu} = 1.0$) as heat transfer takes place principally due to thermal conduction. The effects of Prandtl number have also been investigated in detail and physical explanations are provided for the observed behaviour. New correlations are proposed for the mean Nusselt number $\overline{Nu}$ for both Newtonian and Bingham fluids which are shown to satisfactorily capture the correct qualitative and quantitative behaviour of $\overline{Nu}$ in response to changes in Ra, Pr and Bn.

1. Introduction

Natural convection, i.e. flow caused by temperature-induced density variations, occurs frequently in nature and in technological devices. Even the relatively simple case of natural convection in rectangular enclosures has numerous engineering applications such as in so-called "solar collectors", in heating and preservation of canned foods and in electronic equipment cooling and for energy storage and conservation. As a consequence of these applications, and its geometrical simplicity, a large body of the existing literature [1–3] is available for such flows especially in the case of Newtonian fluids. Interested readers are referred to Ostrach [4] for an extensive review. Although various different configurations of the enclosure problem are possible, one of the most studied cases involves two-dimensional square enclosures where two opposing sides are held isothermally at different temperatures while the other two walls are insulated to ensure adiabatic conditions. When the vertical walls are adiabatic and the lower horizontal wall held at the higher temperature then one has the classical Rayleigh–Bénard configuration [5]. The Rayleigh–Bénard problem has been investigated for a range of different non-Newtonian models including inelastic Generalised Newtonian Fluids (GNF) [6,7], fluids with a yield stress [8–10] and viscoelastic fluids [11]. The present study analyses the case where the horizontal walls are adiabatic and the temperature difference driving the convection comes from the sidewalls as in the classic benchmark paper of de Vahl Davies [1] for Newtonian fluids. Although this configuration has been studied extensively for Newtonian fluids only a relatively limited amount of information is available if the rheological behaviour is more complex. A few papers have investigated variations of this problem for GNF models using both analytical approaches and full numerical simulation of the governing equations. For example Lamsaadi et al. [12,13] has studied the effect of the power-law index in the high Prandtl number limit of tall [12] and also shallow enclosures [13] where the sidewall boundary conditions are constant heat fluxes (rather than isothermal). Barth and Carey [14] utilized more complex GNF models (containing limiting viscosities at low and high shear rates) to study a modified three-dimensional version of the problem (the adiabatic boundary conditions are replaced by a linear variation in temperature to match the experimental conditions of [15]).

For fluids exhibiting a yield stress, i.e. materials that behave as rigid solids for shear stresses lower than a critical yield stress but which flow for higher shear stresses, the recent paper of Vola et al. [16] is the only paper that deals with the sidewall heating case. Vola et al. [16] developed a numerical method to calculate unsteady

* Corresponding author. Tel.: +44 1517944806; fax: +44 1517944848.
E-mail addresses: osmanturan@ktu.edu.tr (O. Turan), n.chakraborty@liv.ac.uk (N. Chakraborty), robpoole@liv.ac.uk (R.J. Poole).

0377-0257/$ – see front matter © 2010 Elsevier B.V. All rights reserved.
doi:10.1016/j.jnnfm.2010.04.013

Nomenclature

c_p	specific heat at constant pressure [J/kg K]
e	relative error [−]
F_s	factor of safety [−]
g	gravitational acceleration [m/s^2]
h	heat transfer coefficient [W/m^2 K]
k	thermal conductivity [W/mK]
L	length and height of the enclosure [m]
q	heat flux [W/m^2]
T	temperature [K]
u_i	ith velocity component [m/s]
U, V	dimensionless horizontal ($U = u_1L/\alpha$) and vertical velocity ($V = u_2L/\alpha$) [−]
ϑ	characteristic velocity [m/s]
x_i	coordinate in ith direction [m]
α	thermal diffusivity [m^2/s]
β	coefficient of thermal expansion [1/K]
δ,δ_{th}	velocity and thermal boundary layer thickness [m]
θ	dimensionless temperature ($\theta = (T - T_C)/(T_H - T_C)$) [−]
μ	plastic viscosity [Ns/m^2]
μ_{yield}	yield viscosity [Ns/m^2]
ν	kinematic viscosity [m^2/s]
ρ	density [kg/m^3]
τ_y	yield stress [N/m^2]
ϕ	general primitive variable
ψ	stream function [m^2/s]

Subscripts

C	cold wall
ext	extrapolated value
eff	effective value
H	hot wall
max	maximum value
ref	reference value
wall	wall value

Special characters

ΔT	difference between hot and cold wall temperature (=($T_H - T_C$)) [K]
$\Delta_{\text{min,cell}}$	minimum cell distance [m]
r	grid expansion ratio [−]

flow of yield stress fluids obeying the Bingham model in a series of geometries. They investigated yield stress effects on the flow pattern and temperature field in square enclosures with differentially heated vertical sidewalls. Their results show that as the yield stress is increased the convection currents diminish and, as a consequence, the mean Nusselt number decreases. At high Bingham numbers convection is essentially absent from the flow and the heat transfer takes place solely by conduction (i.e. the temperature distribution is linear). As the main interest of the work of Vola et al. [16] was primarily in developing the numerical technique the configuration was not investigated in detail and only limited results, for a single Prandtl number (=1), were presented. In the present study the results of Ref. [16] are extended to determine the effects of yield stress on heat and momentum transport for a large range of Rayleigh numbers ($10^3 < Ra < 10^6$) and Prandtl numbers ($0.1 < Pr < 100$). The wide range of Prandtl numbers considered in this study is so that a robust correlation can be achieved. The value of $Pr = 0.1$ is characteristic of molten metals, and, although real yield stress fluids are unlikely to have such low Pr values, it is included here for the sake of completeness.

Without wishing to enter into the ongoing debate about the very existence of a "true" yield stress, it is readily acknowledged that the notion of an apparent yield stress is a very useful engineering empiricism for a wide range of materials [17,18] and from here on this concept will be adopted for the rest of the paper. A number of empirical models have been proposed for describing the interrelation between shear stress and strain rate in yield stress fluids. The most well-known model, and certainly the oldest, is the Bingham model [17] which, in tensorial form, can be expressed as:

$$\underline{\underline{\dot{\gamma}}} = 0, \quad \text{for} \quad \tau \leq \tau_y, \tag{1}$$

$$\underline{\underline{\tau}} = \left(\mu + \frac{\tau_y}{\dot{\gamma}}\right)\underline{\underline{\dot{\gamma}}}, \quad \text{for} \quad \tau > \tau_y, \tag{2}$$

where $\dot{\gamma}_{ij} = \partial u_i/\partial x_j + \partial u_j/\partial x_i$ are the components of the rate of strain tensor $\underline{\underline{\dot{\gamma}}}$, $\underline{\underline{\tau}}$ the stress tensor, τ_y the yield stress, μ the so-called plastic viscosity of the yielded fluid, τ and $\dot{\gamma}$ are evaluated based on the second invariants of the stress and the rate of strain tensors in a pure shear flow respectively, which are given by:

$$\tau = \left[\frac{1}{2}\underline{\underline{\tau}} : \underline{\underline{\tau}}\right]^{1/2}, \tag{3}$$

$$\dot{\gamma} = \left[\frac{1}{2}\underline{\underline{\dot{\gamma}}} : \underline{\underline{\dot{\gamma}}}\right]^{1/2}. \tag{4}$$

O'Donovan and Tanner [19] used the bi-viscosity model to mimic the stress shear-rate characteristics for a Bingham fluid in the following manner:

$$\underline{\underline{\tau}} = \mu_{\text{yield}}\underline{\underline{\dot{\gamma}}}, \quad \text{for} \quad \dot{\gamma} \leq \frac{\tau_y}{\mu_{\text{yield}}}, \tag{5}$$

$$\underline{\underline{\tau}} = \tau_y + \mu\left[\underline{\underline{\dot{\gamma}}} - \frac{\tau_y}{\mu_{\text{yield}}}\right], \quad \text{for} \quad \dot{\gamma} > \frac{\tau_y}{\mu_{\text{yield}}}, \tag{6}$$

where μ_{yield} is the yield viscosity, and μ is the plastic viscosity. In effect this GNF model replaces the solid material by a fluid of high viscosity. O'Donovan and Tanner [19] showed that a value of μ_{yield} equal to $1000\,\mu$ mimics the true Bingham model in a satisfactory manner.

In the present study, the heat transfer rate characteristics in a square enclosure (of dimension L) with differentially heated sided walls filled with a Bingham fluid is compared with the heat transfer rate obtained in the case of Newtonian fluid flows with the same nominal Rayleigh number Ra. The Rayleigh number Ra represents the ratio of the strengths of thermal transports due to buoyancy to thermal diffusion, which is defined in the present study in the following manner:

$$Ra = \frac{\rho^2 c_p g \beta \Delta T L^3}{\mu\, k} = Gr\, Pr \tag{7}$$

where Gr is the Grashof number and Pr is the Prandtl number, which are defined as:

$$Gr = \frac{\rho^2 g \beta \Delta T L^3}{\mu^2} \quad \text{and} \quad Pr = \frac{\mu c_p}{k}. \tag{8}$$

The Grashof number represents the ratio of the strengths of buoyancy and viscous forces while the Prandtl number depicts the ratio of momentum diffusion to thermal diffusion. Alternatively, the Prandtl number can be taken to represent the ratios of hydrodynamic boundary layer to thermal boundary layer thicknesses. These definitions are referred to as "nominal" values as they contain the constant plastic viscosity μ (i.e. are not based on a viscosity representative of the flow). Using dimensional analysis it is possible to show that for Bingham fluids: $Nu = f_1(Ra, Pr, Bn)$ where the

Nusselt number Nu and Bingham number Bn are given by:

$$Nu = \frac{hL}{k} \quad \text{and} \quad Bn = \frac{\tau_y}{\mu}\sqrt{\frac{L}{g\beta\Delta T}} \tag{9}$$

where Nu represents the ratio of heat transfer rate by convection to that by conduction in the fluid in question and the heat transfer coefficient h is defined as:

$$h = \left| -k \left.\frac{\partial T}{\partial x}\right|_{wf} \times \frac{1}{\left(T_{wall} - T_{ref}\right)} \right| \tag{10}$$

where subscript 'wf' refers to the condition of the fluid in contact with the wall, T_{wall} is the wall temperature and T_{ref} is the appropriate reference temperature, which can be taken to be T_C (T_H) for the hot (cold) wall. The Bingham number Bn represents the ratio of yield stress to viscous stresses. In Eq. (9) the viscous straining ($= \mu\sqrt{g\beta\Delta TL}/L$) is estimated based on velocity and length scales given by $\sqrt{g\beta\Delta TL}$ and L respectively. It is worth noting that in Bingham fluid flows, as the viscosity varies throughout the flow, an effective viscosity expressed as $\mu_{eff} = \tau_y/\dot{\gamma} + \mu$ might be more representative of the viscous stress within the flow than the constant plastic viscosity μ. Therefore the Rayleigh, Prandtl and Bingham numbers could have been defined more appropriately if μ_{eff} was used instead of μ. However $\dot{\gamma}$ is expected to show local variations in the flow domain so using a single characteristic value in the definitions of the non-dimensional numbers may not yield any additional benefit in comparison to the definitions given by Eqs. (7)–(9). This subtlety can have important implications when analyzing the effects of yield stress and this issue will be discussed in detail later in the paper. In the present study the effects of Ra, Bn and Pr on Nu are investigated systematically and suitable correlations proposed. However, it is worth noting that in the present study the plastic viscosity μ and yield stress τ_y are taken to be independent of temperature for the sake of simplicity and also due to a lack of reliable data regarding how these effects should be incorporated. Although not ideal this approach seems reasonable as a first step and is consistent with several previous studies on Bingham fluids in the literature [8–10,16]. In addition experimental data [20] for a well-known model yield stress system ("Carbopol") suggests that, in the temperature range 0–90 °C, the yield stress is approximately independent of temperature and the plastic viscosity is only a weakly decreasing function of temperature.

2. Numerical method

The commercial package FLUENT is used to solve the coupled conservation equations of mass, momentum and energy. This commercial package has been used successfully in a number of recent studies to simulate both inelastic power-law fluids [21] and Bingham fluids [22,23]. In this framework, a second-order central differencing scheme is used for the diffusive terms and a second-order up-wind scheme for the convective terms. Coupling of the pressure and velocity is achieved using the well-known SIMPLE (Semi-Implicit Method for Pressure-Linked Equations) algorithm [24]. The convergence criteria in FLUENT were set to 10^{-9} for all the relative (scaled) residuals.

2.1. Governing equations

For the present study steady-state flow of an incompressible Bingham fluid is considered. For incompressible fluids the conservation equations for mass, momentum and energy under steady-state take the following form:

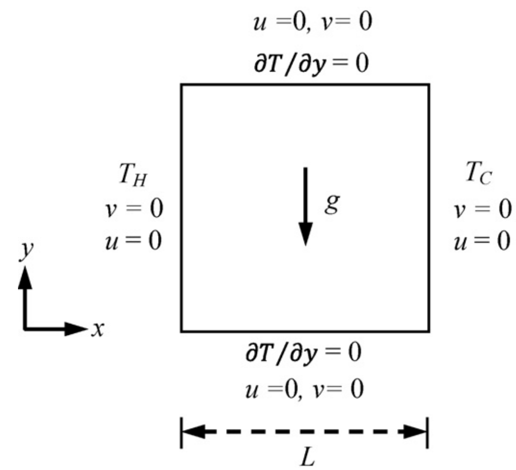

Fig. 1. Schematic diagram of the simulation domain.

Mass conservation equation

$$\frac{\partial u_i}{\partial x_i} = 0 \tag{11}$$

Momentum conservation equations

$$\rho u_j \frac{\partial u_i}{\partial x_j} = -\frac{\partial p}{\partial x_i} + \rho g \delta_{i2}\beta(T - T_C) + \frac{\partial \tau_{ij}}{\partial x_j} \tag{12}$$

Energy conservation equation

$$\rho u_j c_p \frac{\partial T}{\partial x_j} = \frac{\partial}{\partial x_j}\left(k\frac{\partial T}{\partial x_j}\right) \tag{13}$$

where the cold wall temperature T_C is taken to be the reference temperature for evaluating the buoyancy term $\rho g\delta_{i2}\beta(T - T_C)$ in the momentum conservation equations following several previous studies [1–6,16].

The default Bingham model in FLUENT utilizes a bi-viscosity model [19], which is given by Eqs. (5) and (6). The buoyancy effects are accounted for by Boussinesq's approximation but the fluid properties are otherwise assumed to be temperature-independent. The ratio of the yield viscosity (μ_{yield}) to the plastic viscosity (μ) was set to 10^4. In order to assess the sensitivity of the μ_{yield} value, the simulations have been carried out for both $\mu_{\text{yield}} = 10^3\mu$ and $\mu_{\text{yield}} = 10^4\mu$ and quantitative agreement between the results are found to be satisfactory (i.e. maximum deviation in $\overline{Nu}$ is of the order of 0.5%) for all the cases. Given this agreement in what follows only results corresponding to $\mu_{\text{yield}} = 10^4\mu$ are presented. An estimation of a representative effective viscosity μ_{eff} is presented later (see Eq. (28)) in Section 4 of this paper and for all the computations μ_{yield} remained about two orders of magnitude greater than μ_{eff}.

2.2. Boundary conditions

The simulation domain is shown schematically in Fig. 1 where the two vertical walls of a square enclosure are kept at different temperatures ($T_H > T_C$), whereas the other boundaries are considered to be adiabatic in nature. Both velocity components (i.e. u_1 and u_2) are identically zero on each boundary because of the no-slip condition and impenetrability of rigid boundaries. The temperatures for cold and hot vertical walls are specified (i.e. $T(x = 0) = T_H$ and $T(x = L) = T_C$). The temperature boundary conditions for the horizontal insulated boundaries are given by: $\partial T/\partial y = 0$ at $y = 0$ and $y = L$. Here 4 governing equations (1 continuity + 2 momen-

Table 1
Non-dimensional minimum cell distance ($\Delta_{\text{min,cell}}/L$) and grid expansion ratio (r) values.

Grid	M1	M2	M3	M4
	20 × 20	40 × 40	80 × 80	160 × 160
$\Delta_{\text{min,cell}}/L$	4.1325×10^{-3}	1.8534×10^{-3}	8.7848×10^{-4}	4.3001×10^{-4}
r	1.5137	1.2303	1.1092	1.0532

tum + 1 energy) for 4 quantities (u, v, p, T) are solved and thus no further boundary conditions are needed for pressure.

2.3. Grid independency study

The grid independence of the results has been established based on a careful analysis of four different non-uniform meshes M1 (20 × 20), M2 (40 × 40), M3 (80 × 80) and M4 (160 × 160) the details of which are included in Table 1. For some representative simulations (Newtonian ($Bn = 0$) and $Bn = 0.5$ for $Ra = 10^4$ and $Pr = 7$) the numerical uncertainty is quantified here using a grid convergence index (GCI) which is based on Richardson's extrapolation theory [25–27]. For a general primitive variable ϕ the grid-converged value according to Richardson extrapolation is given by: $\phi_{h=0} = \phi_1 + (\phi_2 - \phi_1)/(r^p - 1)$ where ϕ_1 is obtained based on the fine grid and ϕ_2 is the solution based on next level of coarse grid, r is the ratio between the coarse to fine grid spacings and p is the theoretical order of accuracy. Under this framework the GCI is defined as $\text{GCI} = F_s\,|e|\,/(r^p - 1)$ where $e = (\phi_2 - \phi_1)/\phi_1$ is the relative error, F_s is a factor of safety which is often taken to be 3.0. The GCI essentially indicates an error band around the asymptotic numerical value [25–27]. The procedure of the method is given in Ismail and Karatekin [27]. In this analysis the apparent order p was taken to be 2. The numerical uncertainties for the mean Nusselt number $\overline{Nu} = \int_0^L Nu\,dy/L$ and the maximum non-dimensional vertical velocity magnitude on the horizontal mid-plane of the enclosure (V_{max}) are presented for different GCI values in Table 2. For the Newtonian simulations the numerical uncertainty for the maximum dimensionless vertical velocity component on the horizontal mid-plane improved from 0.91% between meshes M2 and M3 to 0.176% between meshes M3 and M4. For the mean Nusselt number the differences between the meshes are essentially negligible. For the Bingham fluid simulations the uncertainty is higher: decreasing from 0.315% to 0.066% for the mean Nusselt number and from 2.506% to 0.74% for the vertical velocity magnitude.

Based on these uncertainties the simulations in the remainder of the paper, unless where otherwise stated, were conducted on mesh M3 which provided a reasonable compromise between high accuracy and computational efficiency. Any simulation in the parameter range in terms of Ra, Pr and Bn explored in the current study using

Table 3
Comparison of present simulation results for Newtonian fluid with the benchmark [1] for $Pr = 0.71$.

		Present study	Benchmark [1]
$Ra = 10^3$	$\overline{Nu}$	1.118	1.118
	Nu_{max}	1.506	1.505
	U_{max}	3.649	3.649
	V_{max}	3.701	3.697
$Ra = 10^4$	$\overline{Nu}$	2.245	2.243
	Nu_{max}	3.531	3.528
	U_{max}	16.179	16.178
	V_{max}	19.655	19.617
$Ra = 10^5$	$\overline{Nu}$	4.520	4.519
	Nu_{max}	7.717	7.717
	U_{max}	34.748	34.730
	V_{max}	68.562	68.590
$Ra = 10^6$	$\overline{Nu}$	8.823	8.800
	Nu_{max}	17.530	17.925
	U_{max}	64.859	64.630
	V_{max}	220.887	219.360

Table 2
Numerical uncertainty for mean Nusselt number $\overline{Nu}$ and maximum non-dimensional vertical velocity component V_{max} on the horizontal mid-plane at $Ra = 10^4$ and $Pr = 7$ for Newtonian and Bingham ($Bn = 0.5$) fluids.

		$\overline{Nu}$			V_{max}		
		M2	M3	M4	M2	M3	M4
Newtonian fluid	ϕ	2.2735	2.2741	2.2742	19.2530	19.6833	19.7670
	ϕ_{ext}		2.27423			19.7949	
	e_{ext} (%)	0.0322	0.0059	0.0015	2.7376	0.5638	0.1409
	GCI (%)	0.0110	0.0018		0.9109	0.1764	
Bingham fluid (Bn = 0.5)	ϕ	1.5109	1.5224	1.5248	8.2614	8.7900	8.9490
	ϕ_{ext}		1.5256			9.0020	
	e_{ext} (%)	0.9636	0.2098	0.0524	8.2271	2.3550	0.5888
	GCI (%)	0.3147	0.0656		2.5057	0.7403	

mesh M3 took typically 8–10 h to converge on a single PC (CPU 3.0 GHz, 2.00 GB of RAM).

2.4. Benchmark comparison

In addition to the aforementioned grid-dependency study, the simulation results for Newtonian fluids have also been compared against the well-known benchmark data of de Vahl Davis [1] for Rayleigh numbers Ra ranging from 10^3 to 10^6 and Prandtl number equal to $Pr = 0.71$. The comparisons between the present simulations results with the corresponding benchmark values are very good and entirely consistent with our grid-dependency studies. The comparison is summarised in Table 3.

The Bingham fluid simulations have been carried out for Bingham numbers Bn ranging from 0 to Bn_{max} where Bn_{max} is the Bingham number at which the mean Nusselt number approaches to unity (i.e. $\overline{Nu} = 1.0$). At $Bn > Bn_{max}$ the solution is independent of the Bingham number Bn because the mean Nusselt number $\overline{Nu}$ remains equal to unity due to heat transfer taking place solely by conduction as the fluid flow dies out in the cavity. It is important to note that Vola et al. [16] did not report the values of Bn but simply provided the values of yield stress τ_y. According to the present definition of Bingham number Bn (see Eq. (9)) the values of Bn for $Ra = 10^4, 10^5$ and 10^6 cases in Table 5 of Vola et al. [16] turn out to be 3, 0.95 and 0.3 respectively. For these limited cases the present simulation results for the above values of Bn and Ra for $Pr = 1.0$ were in reasonable agreement with the values reported by Vola et al. [16] (maximum difference in $\overline{Nu}$ is smaller than 3% for example).

3. Scaling analysis

A scaling analysis is performed to elucidate the anticipated effects of Rayleigh number, Prandtl number and Bingham number on the Nusselt number for yield stress fluids. The wall heat flux q can be scaled as:

$$q \sim k\frac{\Delta T}{\delta_{th}} \sim h\,\Delta T \tag{14}$$

which gives rise to the following relation:

$$Nu \sim \frac{hL}{k} \sim \frac{L}{\delta_{th}} \quad \text{or} \quad Nu \sim \frac{L}{\delta} f_2(Pr, Bn) \tag{15}$$

where the thermal boundary layer thickness δ_{th} is related to the hydrodynamic boundary layer thickness δ in the following manner: $\delta/\delta_{th} \sim f_2(Pr, Bn)$ where $f_2(Pr, Bn)$ is a function of Prandtl and Bingham numbers (i.e. Pr and Bn), which is expected to increase with increasing Prandtl number. In order to estimate the hydrodynamic boundary layer thickness δ, a balance of inertial and viscous forces in the vertical direction (i.e. y-direction) is considered:

$$\rho\frac{\vartheta^2}{L} \sim \frac{\tau}{\delta} \tag{16}$$

where ϑ is a characteristic velocity scale. For Bingham fluids the shear stress τ can be estimated as: $\tau \sim \tau_y + \mu\,\vartheta/\delta$, which upon substitution in Eq. (16) gives:

$$\rho\frac{\vartheta^2}{L} \sim \left(\tau_y + \mu\frac{\vartheta}{\delta}\right)\frac{1}{\delta}. \tag{17}$$

Using Eq. (17) the hydrodynamic boundary layer thickness can be estimated as:

$$\delta = \frac{1}{2}\frac{\tau_y L}{\rho\,\vartheta^2} + \frac{1}{2}\frac{L}{\rho\,\vartheta^2}\sqrt{\tau_y^2 + 4\rho\frac{\vartheta^3}{L}\mu}. \tag{18}$$

For natural convection the flow is induced by the buoyancy force and thus the equilibrium of inertial and buoyancy forces gives:

$$\frac{\vartheta^2}{L} \sim g\beta\Delta T. \tag{19}$$

This balance leads to an expression for the characteristic velocity scale:

$$\vartheta \sim \sqrt{g\beta\Delta T L} \tag{20}$$

which can be used in Eq. (18) to yield:

$$\delta \sim \frac{\mu/\rho}{\sqrt{g\beta\,\Delta T\,L}}\left[\frac{Bn}{2} + \frac{1}{2}\sqrt{Bn^2 + 4\left(\frac{Ra}{Pr}\right)^{1/2}}\right] \tag{21}$$

where Ra and Bn are given by Eqs. (7) and (9) respectively. This scaling gives rise to the following expression for the thermal boundary layer thickness δ_{th}:

$$\delta_{th} \sim \min\left[L, \frac{L\,Pr^{1/2}}{f_2(Bn, Pr)Ra^{1/2}}\left[\frac{Bn}{2} + \frac{1}{2}\sqrt{Bn^2 + 4\left(\frac{Ra}{Pr}\right)^{1/2}}\right]\right]. \tag{22}$$

The above expression accounts for the fact the thermal boundary layer thickness becomes of the order of the enclosure size L under very high values of Bn when the Bingham fluid acts essentially as a solid material. Eq. (22) suggests that δ_{th} decreases with increasing Ra, which acts to increase the wall heat flux. Substitution of Eq. (22) into Eq. (15) yields:

$$\overline{Nu} \sim Max\left[1.0, \quad \frac{Ra^{1/2}/Pr^{1/2}}{\left[\frac{Bn}{2} + \frac{1}{2}\sqrt{Bn^2 + 4\left(\frac{Ra}{Pr}\right)^{1/2}}\right]} f_2(Pr, Bn)\right]. \tag{23}$$

The scaling predictions provide useful insight into the anticipated behaviour of Nu in response to variations of Ra, Pr and Bn. The analysis suggests that Nu is expected to decrease with increasing Bn for a given value of Ra whereas Nu increases with increasing Ra for a given value of Bn. It is also important to note that the Nusselt number behaviour for Newtonian fluids can be obtained by setting $Bn = 0$ in Eq. (23). Doing so gives $\overline{Nu} \sim Ra^{0.25} f_2(Pr)/Pr^{0.25}$ for Newtonian fluids whereas Berkovsky and Polevikov [28] proposed the correlation $\overline{Nu} = 0.18[Ra\,Pr/(0.2 + Pr)]^{0.29}$. Given the simplicity of the above scaling analysis it is not surprising that a small quantitative difference between the value of exponent of Ra between the prediction of Eq. (23) and the correlation function exists (0.25 cf. 0.29). However, the qualitative trends are nicely captured by the scaling relations.

4. Results and discussion

4.1. Rayleigh number effects

The variation of mean Nusselt number $\overline{Nu}$ with normalised vertical distance y/L is shown in Fig. 2. The results show that $\overline{Nu}$ increases with Ra for both Newtonian and Bingham fluids, which is consistent with the scaling analysis discussed earlier (see Eq. (23)). In addition it can be observed that the values of $\overline{Nu}$ for Bingham fluids are smaller than that obtained in the case of Newtonian fluids with the same nominal Rayleigh number Ra. Again this effect is also in agreement with the scaling estimate of Nusselt number given by Eq. (23).

It is instructive to look into the distributions of the dimensionless temperature θ and vertical velocity component V to explain the variation of $\overline{Nu}$ with Bn shown in Fig. 2. Only the vertical velocity component is shown as the horizontal velocity component is of the same order for square enclosures. The distributions of θ and

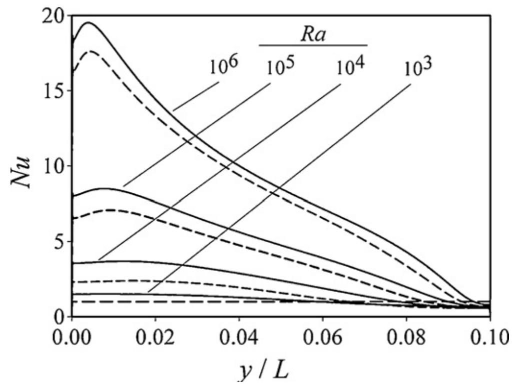

Fig. 2. Variation of *Nu* with normalised vertical distance along the hot wall for $Pr = 7$ (—) Newtonian case and (- - -) Bingham fluid case (for $Bn = 0.5$).

V for both Newtonian and Bingham fluids (at $Bn = 0.5$) along the horizontal mid-plane are shown in Fig. 3 for different values of Rayleigh number Ra. At $Ra = 10^3$ the distribution of θ is completely linear and the vertical velocity component is essentially negligible due to very weak flow as the effects of buoyancy forces are dominated by viscous effects. Under this circumstance, the heat transfer takes place entirely by conduction across the enclosure. The effects of buoyancy force strengthens relative to the viscous force with increasing Ra for a given set of values of Bn and Pr, which in turn augments heat transfer by convection due to stronger buoyancy-driven flow with higher vertical velocity magnitude. This effect is clearly evident from Fig. 3, which indicates that the vertical velocity magnitude does indeed increase with increasing Ra for both Newtonian and Bingham fluids. The distribution of non-dimensional temperature becomes increasingly non-linear with the strengthening of convective transport for higher values of Ra for both Newtonian and Bingham fluids. This strengthening is also apparent in Fig. 4a and b where the contours of stream function and non-dimensional temperature are shown for both Newtonian and Bingham fluids (at $Bn = 0.5$) for different values of Ra. It is evident from Fig. 4a and b that the isotherms become increasingly curved with increasing Rayleigh number due to a strong convective current within the enclosure, while temperature contours are parallel to the wall due to the conduction-dominated thermal transport at the lowest Rayleigh number. It can be discerned from Fig. 4b that the thermal boundary layer thickness on the side walls decreases with increasing Ra for both Newtonian and Bingham fluids, which is consistent with the trend predicted by our scaling estimate of δ_{th} (see Eq. (22)).

The “unyielded” zones (defined using the criteria proposed in Ref. [18]: zones of fluid where $|\tau| \le \tau_y$) are also shown in Fig. 4a. It is important to note that these zones are not really “unyielded” in the true sense as pointed out by Mitsoulis and Zisis [29]. In the present study a bi-viscosity approximation is used to model the Bingham fluid flow so there will always be flow within these essentially very high viscosity regions – regions of extremely slowly moving fluid (Mitsoulis and Zisis [29] called them “apparently unyielded regions (AUR)”). It is important to stress that the small islands of AUR within the centre of the enclosure alter significantly with increasing values of μ_{yield} (shown in Fig. 4a for $\mu_{\text{yield}} = 10^4\mu$) while the mean Nusselt number, the stream function and the zones of AUR at the corners of the enclosure are independent of μ_{yield} for $\mu_{\text{yield}} \ge 10^3\mu$. For a given value of τ_y the zones with very low shear rate, which satisfy $|\tau| \le \tau_y$, are expected to shrink with an increase in μ_{yield}, as the strain rate field remains independent of μ_{yield} for the simulations considered here. As the AUR zones are dependent on the choice of μ_{yield}, any in depth discussion of their significance is not considered to be worthwhile for this paper. The streamlines in the bottom right-hand corner of the enclosure are also shown within Fig. 4a (as a zoomed insert), which highlight the approximate size of the corner eddy. This corner vortex diminishes in size with increasing Rayleigh number.

4.2. Bingham number effects

The variations of the mean Nusselt number $\overline{Nu}$ with Bingham number Bn are shown in Fig. 5 for nominal values of Rayleigh num-

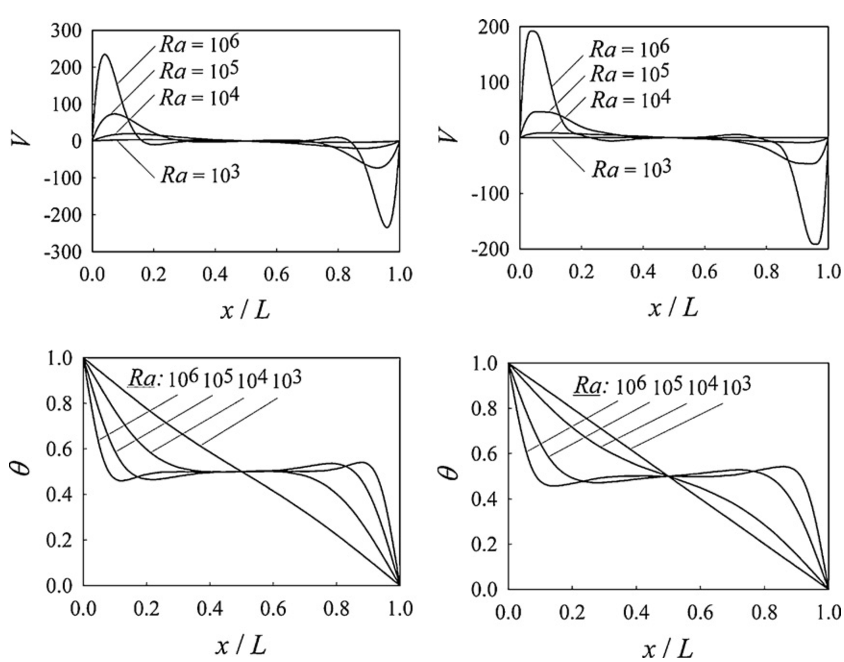

Fig. 3. Variations of non-dimensional temperature θ and vertical velocity component V along the horizontal mid-plane for Newtonian case (left column) and Bingham fluid case (for $Pr = 7$).

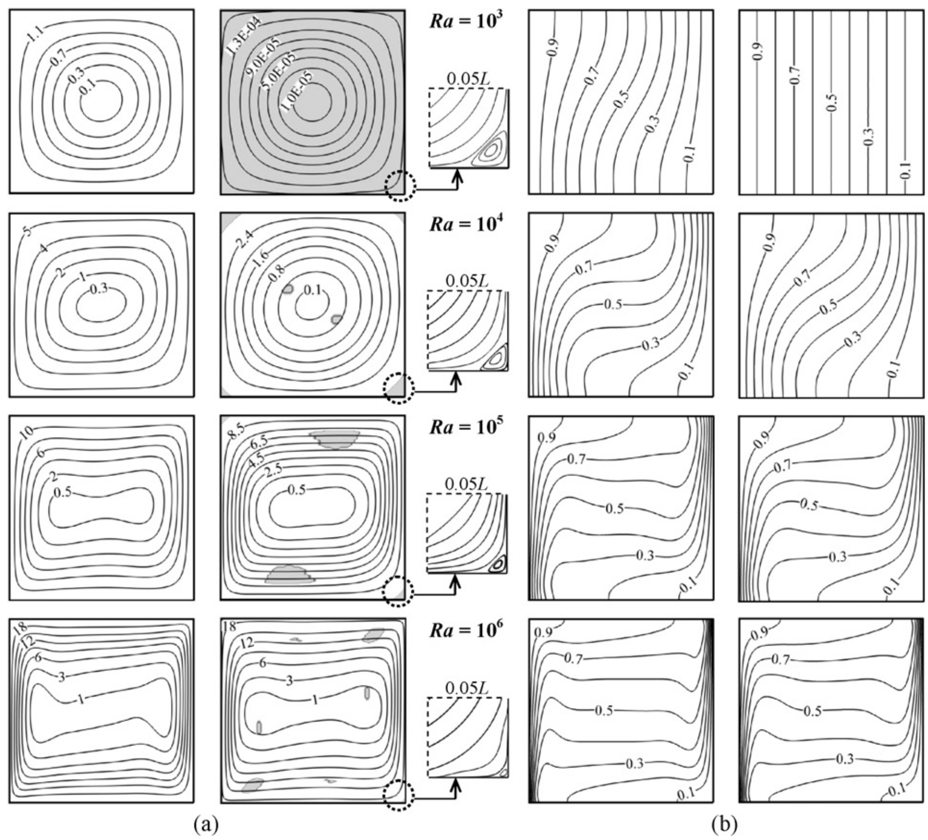

Fig. 4. (a) Contours of non-dimensional stream functions (ψ/α) and unyielded zones (gray) including a zoomed inset of qualitative features of corner vortex and (b) contours of non-dimensional temperature θ for Newtonian case (left column) and Bingham fluids case (for Bn = 0.5, right column) at Pr = 7.

ber $Ra = 10^3$, 10^4, 10^5 and 10^6. The Prandtl number Pr is taken to be 7.0 as this value represents a realistic value of Pr for incompressible fluids. It is clear from Fig. 5 that $\overline{Nu}$ decreases with increasing Bn, and ultimately the value of $\overline{Nu}$ settles to unity, as demonstrated in Fig. 5. This behaviour is consistent with earlier results by Vola et al. [16]. It is worth noting that heat transfer due to pure conduction yields a Nusselt number value equal to $\overline{Nu} = 1.0$ (i.e. $q \sim k\Delta T/L \sim h\Delta T$ or $\overline{Nu} = hL/k \sim 1.0$) so the value of $\overline{Nu}$ essentially indicates the extent of deviation from the pure conduction simulation results. For high values of Bingham number Bn, the viscous force more readily overcomes the buoyancy force and as a result of this, no significant flow is induced within the enclosure. This result is clearly apparent from Fig. 6a and b where the effects of Bn on the distributions of non-dimensional temperature and vertical velocity component along the horizontal mid-plane are shown for $Ra = 10^4$ and $Ra = 10^6$ respectively. It can be seen from Fig. 6a and b that the temperature profiles become linear and the vertical component of velocity disappears for higher values of Bn (i.e. $Bn \geq Bn_{\max}$) when the mean Nusselt number approaches to unity (i.e. $\overline{Nu} = 1.0$) (see Fig. 5). This behaviour can further be understood by comparing the contours of stream function and non-dimensional temperature shown in Fig. 7a and b for different values of Bn at $Ra = 10^4$ and $Ra = 10^6$. Both Figs. 6 and 7 suggest that the effects of convection (i.e. fluid flow) within the enclosure decreases with increasing Bn and the Bingham fluid starts to behave as a solid for $Bn \geq Bn_{\max}$: the fluid velocities drop to such low values that for all practical purposes the fluid is essentially stagnant. The values of Bingham number either close to or greater than Bn_{max} will henceforth be referred to as large values of Bingham number for the rest of the paper.

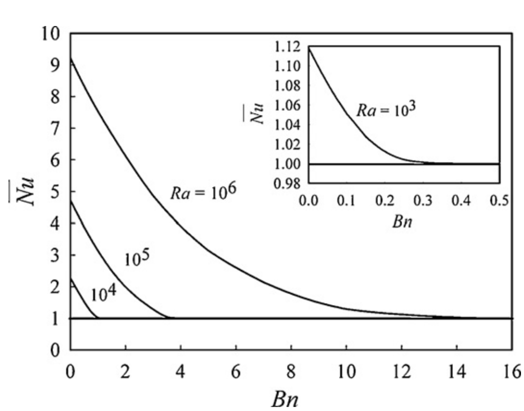

Fig. 5. The interrelation between the mean Nusselt number $\overline{Nu}$ and Bingham number Bn for different values of Rayleigh number at Pr = 7.

In the absence of flow in the enclosure, heat transfer takes place due to conduction and thus the isotherms remain parallel to the side walls (see Fig. 7) conforming to the pure conduction solution. This effect is reflected by $\overline{Nu} = 1.0$ for $Bn \geq Bn_{\max}$ in Fig. 5. The effects of buoyancy force strengthen in comparison to the viscous effects with increasing Ra. As a result of the stronger buoyancy effects, the Bingham number at which $\overline{Nu}$ approaches to unity (i.e. $Bn = Bn_{max}$) increases with increasing Ra. It has already been mentioned that the situation when buoyancy effects become insignificant and heat transfer is purely due to thermal conduction is given by $\overline{Nu} = 1.0$. Thus, the value of Bingham number Bn at which $\overline{Nu}$ approaches to $\overline{Nu} = 1.0$ is a critical Bingham number Bn_{max} which essentially indicates that natural convection effects are important (unimportant) for $Bn < Bn_{\max}$ ($Bn \geq Bn_{\max}$).

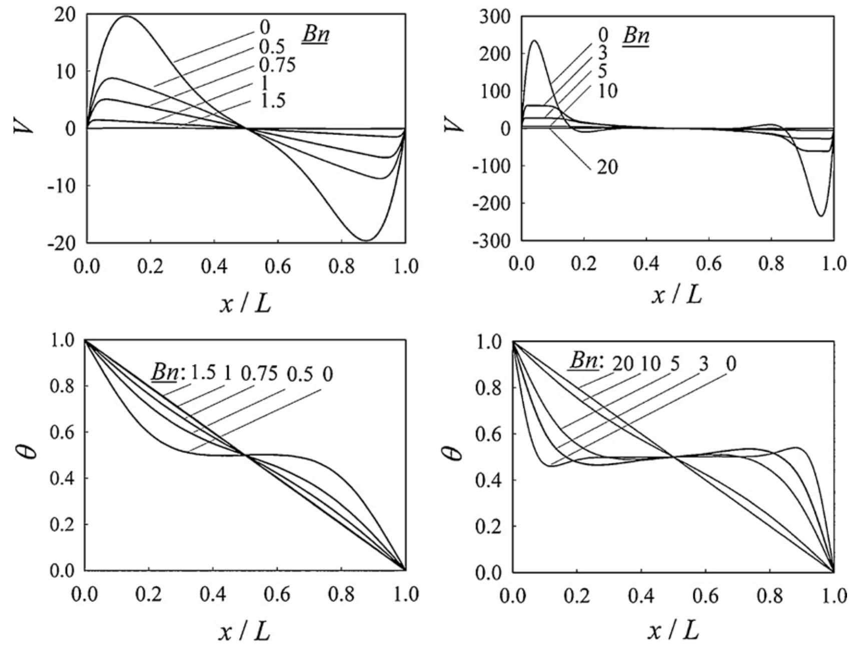

Fig. 6. Variations of non-dimensional temperature θ and vertical velocity component V along the horizontal mid-plane for different values of the Bingham number Bn in the case of $Ra = 10^4$ (left column) and $Ra = 10^6$ (right column) ($Pr = 7$).

4.3. Prandtl number effects

In this section, Prandtl number effects are investigated for both Newtonian and Bingham fluid cases for Prandtl numbers ranging from $Pr = 0.1$ to 100 in the Rayleigh number range $Ra = 10^4$–10^6. The lower Ra bound is close to the onset of significant convection effects whereas our upper bound choice reflects our desire to ensure steady-state two-dimensional simulations retain physical significance. Based on the simulation results new correlations for $\overline{Nu}$ are suggested for both Newtonian and Bingham fluids in terms of Rayleigh number Ra, Prandtl number Pr and Bingham number Bn.

4.3.1. Newtonian fluids

The variation of $\overline{Nu}$ with Pr for Newtonian fluids is shown in Fig. 8 which indicates that $\overline{Nu}$ increases with increasing Pr. It can be seen from Fig. 8 that the results for Newtonian fluids are consistent with earlier numerical results [30] whereas the simulation results deviate somewhat from the correlation proposed by Berkovsky and Polevikov [28] ($\overline{Nu} = 0.18\left[Ra\ \ Pr/(0.2 + Pr)\right]^{0.29}$). Moreover, it is clear that Pr has an important influence on $\overline{Nu}$ for small values ($Pr \ll 1$). However, $\overline{Nu}$ is relative insensitive to Pr for high Prandtl number values. In the present configuration, the relative strengths of inertial, viscous and buoyancy forces determine the flow behaviour. For small values of Pr the thermal boundary layer thickness remains much greater than the hydrodynamic boundary layer thickness. As a result of this difference, the transport behaviour in the majority of the domain is governed by the inertial and buoyancy forces. In contrast, for large values of Pr the hydrodynamic boundary layer thickness remains much greater than the thermal boundary later thickness thus the transport characteristics are primarily driven by buoyancy and viscous forces (see the scaling analysis by Bejan [5] for example). For $Pr \ll 1$, an increase in Pr decreases the thermal boundary layer thickness in comparison to the hydrodynamic boundary layer thickness. This change essentially acts to increase the heat flux which is reflected in the increasing Nusselt number. In the case of $Pr \gg 1$, a change in Prandtl number principally modifies the relative balance between viscous and buoyancy forces so the heat transport in the thermal boundary layer gets only marginally affected. This modification is reflected in the weak Prandtl number dependence of $\overline{Nu}$ for large values of Pr (i.e. $Pr \gg 1$) in Fig. 8.

In the case of Newtonian fluids, the average Nusselt number $\overline{Nu}$ is expressed in terms of an algebraic function of Ra and Pr:

$$\overline{Nu} = a\,Ra^m \left(\frac{Pr}{1 + Pr}\right)^n. \tag{24}$$

The values of coefficients a, m and n were determined using an iterative minimisation function of a commercial software package with the parameters from the Berkovsky and Polevikov [28] fit used as initial values (giving $a = 0.162$, $m = 0.293$ and $n = 0.091$). Including more free parameters resulted in only marginal improvements to the fit. As Fig. 8 shows the correlation given by Eq. (24) predicts the mean Nusselt number $\overline{Nu}$ obtained from the simulation data satisfactorily for different values of Ra and Pr. In addition Eq. (24) offers an improvement over the correlation of Berkovsky and Polevikov [28] which, for high Prandtl numbers, over-predicts the mean Nusselt number (differences of the order of 10%).

4.3.2. Bingham fluids

In order to demonstrate the effects of Pr on $\overline{Nu}$ for Bingham fluids, the variations of $\overline{Nu}$ with different values of Pr and Bn at a nominal Rayleigh number value $Ra = 10^5$ are shown in Fig. 9. It is evident from Fig. 9 that $\overline{Nu}$ decreases with increasing Pr for large values of Bn unlike the situation for Newtonian fluids. In contrast, the mean Nusselt number $\overline{Nu}$ increases with increasing Pr for very small values of Bn, which is consistent with the behaviour obtained for Newtonian fluids (see Fig. 8). Moreover, the value of Bingham number Bn_{max} for which $\overline{Nu}$ approaches to unity decreases with increasing Pr. The same qualitative behaviour is also observed for other values of Ra and thus is not shown here for the sake of conciseness. In order to explain this observation it is instructive to examine

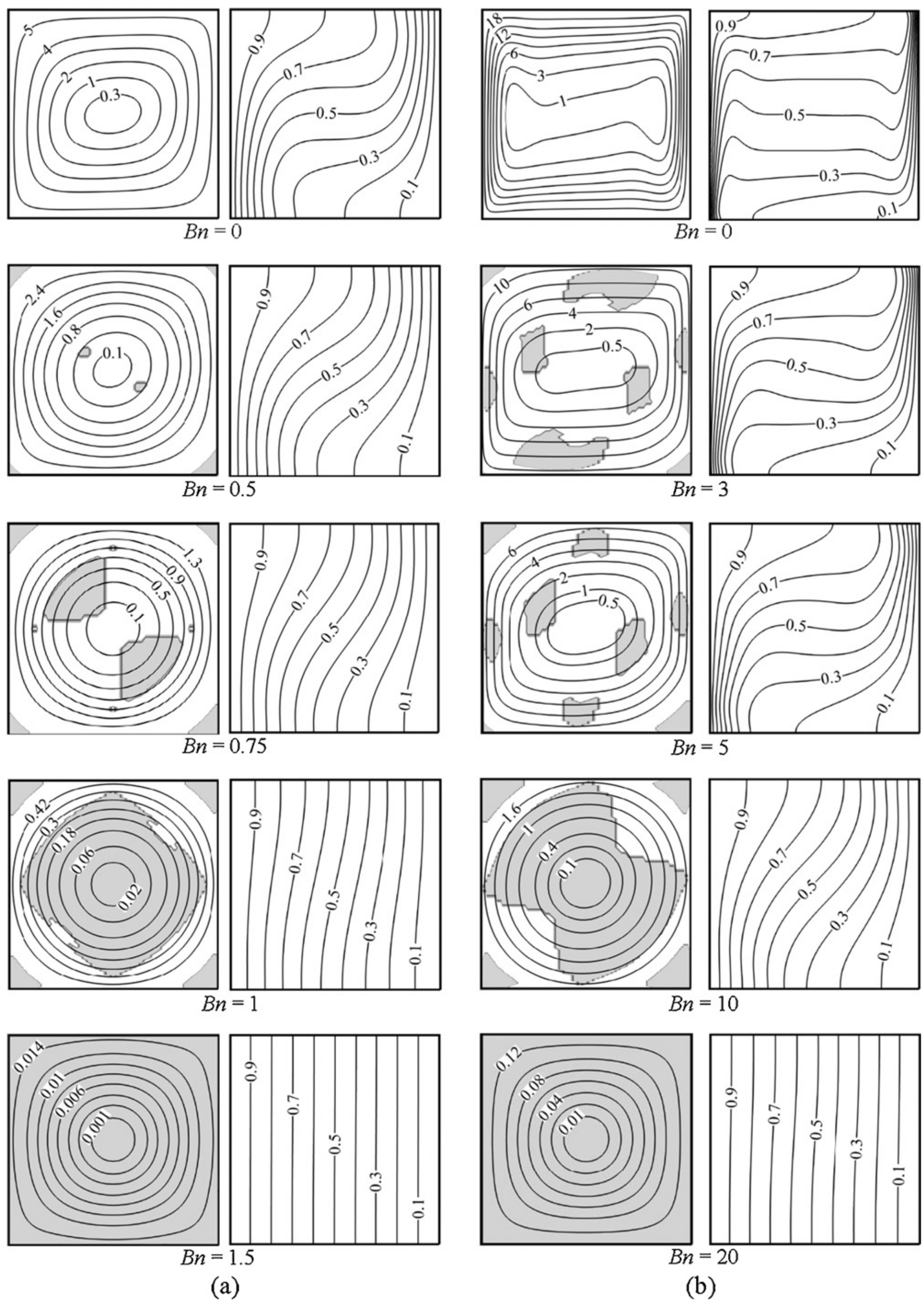

Fig. 7. Contours of non-dimensional stream functions (ψ/α) (left column) with unyielded zones (gray), and non-dimensional temperature θ (right column) for different values of Bn at $Pr = 7$, (a) $Ra = 10^4$ and (b) $Ra = 10^6$.

the non-dimensional temperature contours at various values of Pr, which are presented in Fig. 10 for a range of values of Bn at a nominal Rayleigh number $Ra = 10^5$. It can be observed from Fig. 10 that the effects of convection disappear for smaller values of Bn for higher values of Pr, which is consistent with the observations based on Fig. 9. This variation clearly demonstrates that the Bingham number at which the fully-conduction regime starts depends on Pr for a given value of Ra. From the foregoing it can be concluded that the effects of Pr on natural convection at a given value of Ra are not fully independent of Bn. This inference is an artefact of how the nominal Ra is defined in the present analysis (see Eq. (7)). In the case of natural convection in Bingham fluids the use of an effective viscosity μ_{eff} instead of the constant plastic viscosity μ in the definition of Rayleigh number would have been more appropriate. One way of estimating an "effective" viscosity is described below:

$$\mu_{eff} = \tau_y/\dot{\gamma} + \mu \tag{25}$$

which can be scaled as:

$$\mu_{eff} \sim \tau_y \delta/\vartheta + \mu. \tag{26}$$

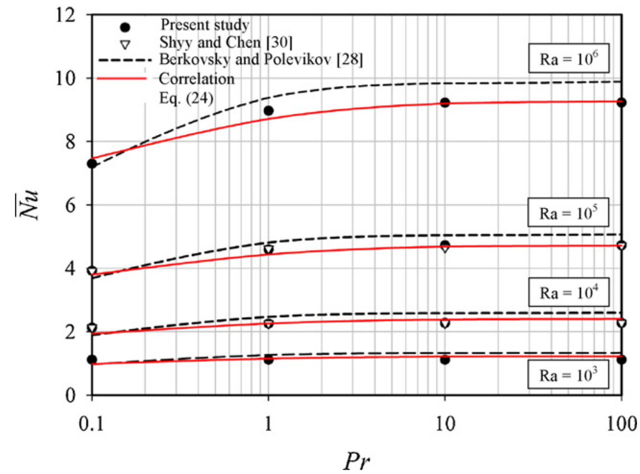

Fig. 8. Variation of mean Nusselt number $\overline{Nu}$ with Rayleigh Ra and Prandtl Pr numbers for Newtonian fluids.

Using Eq. (21) in Eq. (26) yields:

$$\mu_{eff} \sim \mu \left\{ Bn \left[\frac{Bn\mu}{2\rho\vartheta L} + \frac{\mu}{2\vartheta L\rho} \sqrt{Bn^2 + 4\frac{\rho\,\vartheta\, L}{\mu}} \right] \right\} + \mu. \tag{27}$$

Using velocity scale $\vartheta \sim \sqrt{g\beta\,\Delta T\,L}$ (Eq. (20)) gives:

$$\mu_{eff}/\mu \sim \left\{ Bn \left[\frac{Bn}{2Gr^{1/2}} + \frac{1}{2Gr^{1/2}} \sqrt{Bn^2 + 4Gr^{1/2}} \right] \right\} + 1. \tag{28}$$

Based on Eq. (27) an effective Grashof number Gr_{eff} can be defined as:

$$Gr_{eff} = \frac{\rho^2 g\beta\Delta T L^3}{\mu_{eff}^2} = Gr\left[\left\{ Bn \left[\frac{Bn}{2Gr^{1/2}} + \frac{1}{2Gr^{1/2}} \sqrt{Bn^2 + 4Gr^{1/2}} \right] \right\} + 1 \right]^{-2}. \tag{29}$$

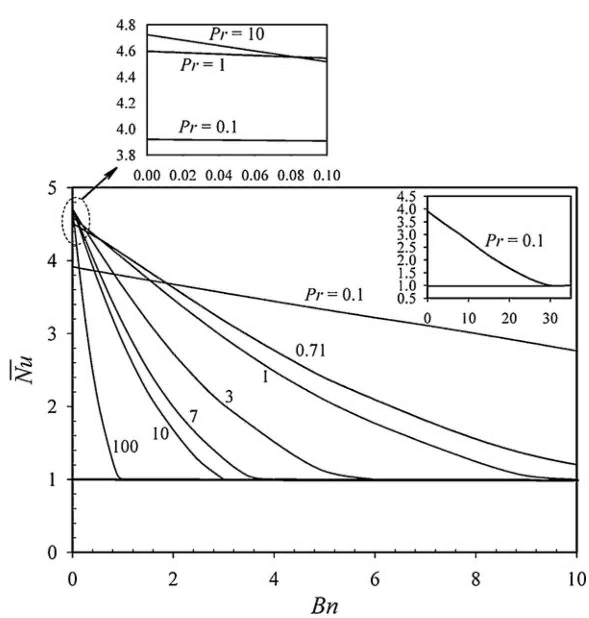

Fig. 9. Variations of mean Nusselt number $\overline{Nu}$ with Prandtl number for Bingham fluids at $Ra = 10^5$.

The variation of Gr_{eff} with Pr according to Eq. (29) is shown in Fig. 11 for different values of Bn. The case with $Bn = 0$ corresponds to the Newtonian case and Fig. 11 suggests that the effective Grashof number decreases with increasing Pr for a given value of Ra and this drop becomes increasingly rapid with increasing values of Bn. For large values of Bn the effects of the buoyancy force becomes increasingly weak in comparison to the viscous effects with increasing Pr when Ra is held constant. This reduced buoyancy force relative to the viscous force gives rise to a weakening of convective transport which acts to decrease $\overline{Nu}$ with increasing Pr. This effect is relatively weak for small values of Bn where an increase in Prandtl number acts to reduce the thermal boundary layer thickness which in turn acts to increase the heat transfer rate as discussed earlier in the context of Newtonian fluids. In contrast, for large values of Bn, the effects of thinning of the thermal boundary layer thickness with increasing Pr is superseded by the reduction of convective transport strength due to a smaller value of the effective Grashof number. This reduction gives rise to a decrease in $\overline{Nu}$ with increasing values of Pr (for a given value of Ra) when the Bingham number assumes large values. Eventually this gives rise to the beginning of the conduction-dominated regime for smaller values of Bn_{max} for higher Pr values as shown in Fig. 10 (for constant Ra). As a consequence Bn_{max} depends on both Rayleigh and Prandtl numbers, and Bn_{max} increases with increasing Rayleigh number, whereas it decreases with increasing Prandtl number. These results are shown in Table 4 where the variations of Bn_{max} with Ra and Pr are summarised.

Once again useful insight into this behaviour can also be obtained using a scaling analysis. According to Eq. (15) $\overline{Nu}$ can be estimated as: $\overline{Nu} \sim L f_2(Pr, Bn)/\delta$, which leads to the following expression according to Eq. (22) when $\overline{Nu}$ approaches to unity

$$f_2(Pr, Bn_{\max}) \frac{Ra^{1/2}}{Pr^{1/2}} \sim \left[\frac{Bn_{\max}}{2} + \frac{1}{2}\sqrt{Bn_{\max}^2 + 4\left(\frac{Ra}{Pr}\right)^{1/2}} \right] \tag{30}$$

which can be manipulated to yield:

$$Bn_{\max} \sim f_2(Pr, Bn_{\max}) \frac{Ra^{1/2}}{Pr^{1/2}} - \frac{1}{f_2(Pr, Bn_{\max})}. \tag{31}$$

Eq. (31) demonstrates that Bn_{max} depends on both Ra and Pr, which is consistent with the simulation results. In the present study the mean Nusselt number $\overline{Nu}$ is taken to be of the following form in the ranges given by $0.1 \le Pr \le 100$, $10^4 \le Ra \le 10^6$ and $0 \le Bn \le Bn_{max}$:

$$\overline{Nu} = 1 + \frac{A\,Ra^{1/2}}{\left[\frac{Bn}{2} + \frac{1}{2}\sqrt{Bn^2 + 4\left(\frac{Ra}{Pr}\right)^{1/2}} \right]} \left[1 - \frac{Bn}{Bn_{\max}} \right]^b \tag{32}$$

so that

$$\lim_{Bn \to Bn_{\max}} \overline{Nu} = 1 + \frac{A\,Ra^{1/2}}{\left[\frac{Bn_{\max}}{2} + \frac{1}{2}\sqrt{Bn_{\max}^2 + 4\left(\frac{Ra}{Pr}\right)^{1/2}} \right]} \times \left[1 - \frac{Bn_{\max}}{Bn_{\max}} \right]^b = 1.0 \tag{33}$$

where A, b and Bn_{max} are input parameters in the correlation which need to be determined from the numerical results. The parameter A is chosen in such a manner that Eq. (33) becomes identically equal to Eq. (24) when the Bingham number Bn goes to zero. This yields the following expression for A:

$$A = a\,Ra^{m-0.25} \frac{Pr^{n-0.25}}{(1+Pr)^n} - \frac{1}{Ra^{0.25}Pr^{0.25}}. \tag{34}$$

The simulation results suggest that the parameter b depends on both Ra and Pr and it has been found that the variation of b with Ra

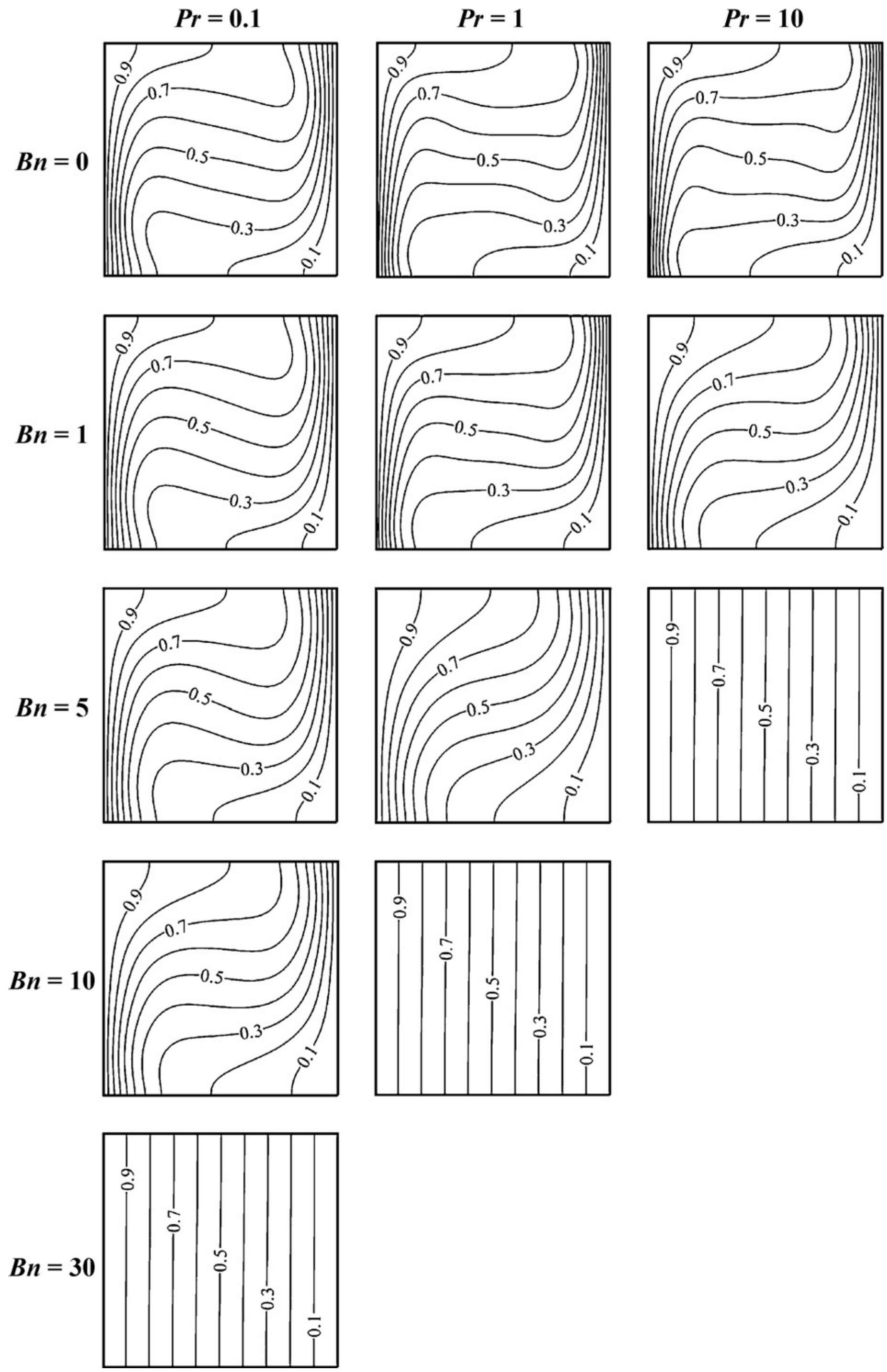

Fig. 10. Contours of non-dimensional temperature θ for different values of Prandtl and Bingham numbers at $Ra = 10^5$.

and *Pr* can be accurately expressed with the help of the following power-law:

$$b = 0.42Ra^{0.13}Pr^{0.12}. \quad (35)$$

It has been discussed earlier that the value of Bn_{max} is dependent on *Ra* and *Pr* and here the value of Bn_{max} is estimated by fitting the simulation results, which leads to:

$$Bn_{\max} = 0.019Ra^{0.56}Pr^{-0.46}. \quad (36)$$

The correlation is applicable for any Bingham fluid in the following range of Prandtl and Rayleigh numbers: $0.1 \le Pr \le 100$, $10^4 \le Ra \le 10^6$. The predictions of the correlation given by Eq. (32) is compared with our numerical data obtained from the present simulation data in Fig. 12, which demonstrates that the correlation given by Eq. (32) satisfactorily captures both qualitative and quantitative variations of $\overline{Nu}$ with *Bn* for the range of *Ra* and *Pr* analysed in this study. However, the agreement between the prediction of Eq. (32) and the simulation results deteriorates for smaller values of Prandtl number (i.e. $Pr = 0.1$). For example, the correlation given

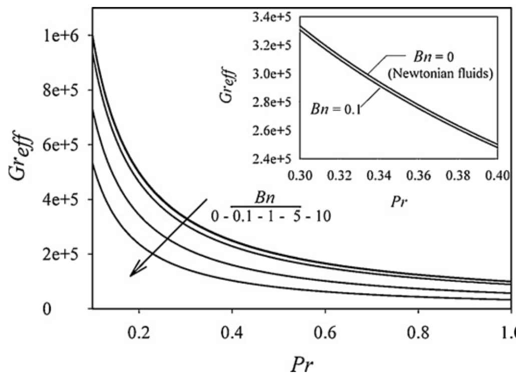

Fig. 11. Variation of effective Grashof number Gr_{eff} with Prandtl number Pr at $Ra = 10^5$.

by Eq. (32) under predicts $\overline{Nu}$ for small values of Bn for $Ra = 10^4$ and $Pr = 0.1$ and this disagreement originates principally due to the limitation of the correlation of the Newtonian fluids (Eq. 24) in predicting $\overline{Nu}$ for small values of Pr (see Fig. 8), which in turn affects the prediction of Eq. (32) through the value of A (see Eq. 34). However, the implications of this inaccuracy is not likely to be severe because all known yield stress fluids in practical applications are likely to have Pr significantly greater than 0.1.

Table 4
Values of Bn_{max} at different values of Ra and Pr.

Pr	$Ra = 10^4$	$Ra = 10^5$	$Ra = 10^6$
0.1	10	35	125
1	3	10	45
10	1	4	15
100	0.3	1	5

5. Conclusions

In this study, the heat transfer characteristics of steady laminar natural convection of yield stress fluids obeying the Bingham model in a square enclosure with differentially heated side walls have been numerically studied. The effects of Rayleigh number Ra, Prandtl number Pr and Bingham number Bn on heat and momentum transport have been systematically investigated. It is found that the mean Nusselt number $\overline{Nu}$ increases with increasing values of the Rayleigh number for both Newtonian and Bingham fluids. However the Nusselt numbers obtained for Bingham fluids are smaller than those obtained in the case of Newtonian fluids with the same values of nominal Rayleigh number. The Nusselt number was found to decrease with increasing Bingham number, and, for large values of Bingham number, the value of mean Nusselt number settled to unity (i.e. $\overline{Nu} = 1$) as the heat transfer took place princi-

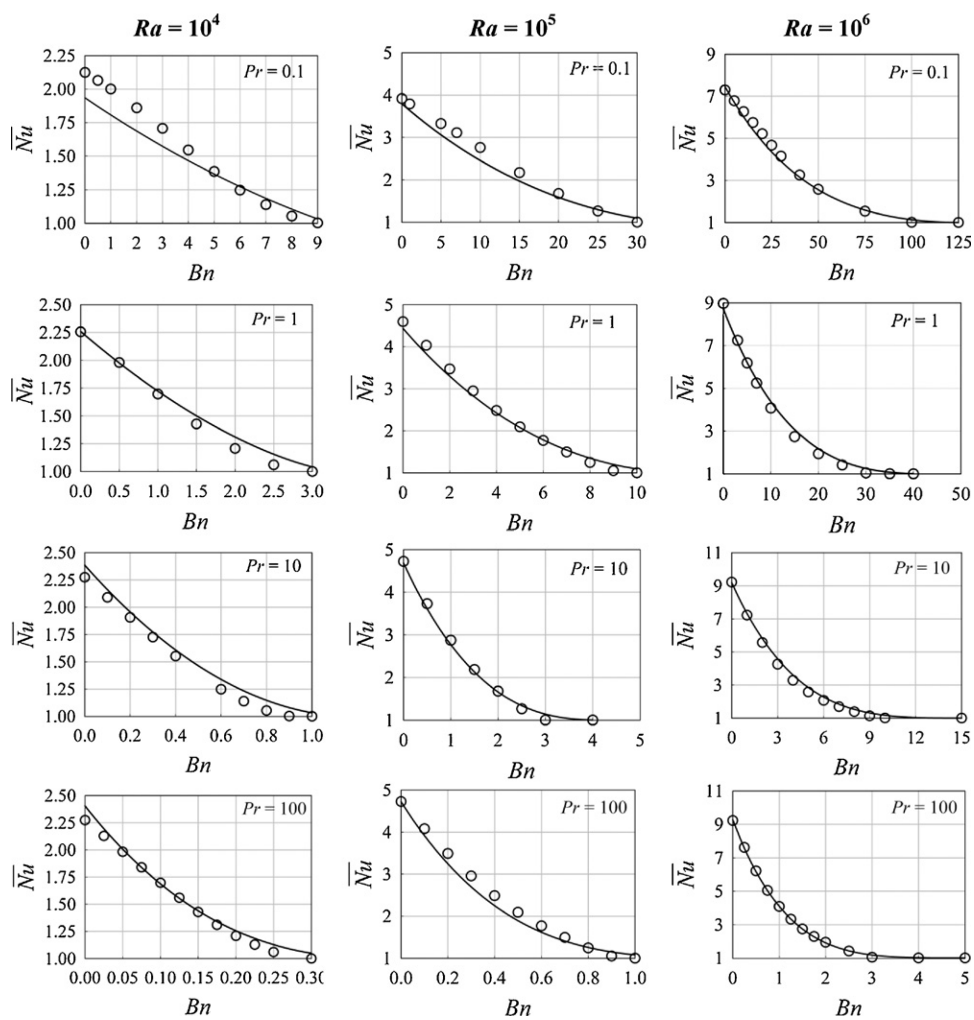

Fig. 12. Comparison of the prediction of the correlation (—) given by Eq. (32) and simulation results (○).

pally by conduction. The conduction-dominated regime occurs at higher values of Bn for increasing values of Ra.

The simulation results show that the mean Nusselt number $\overline{Nu}$ increases with increasing Pr for Newtonian fluids and low Bingham number flows for a given value of the Rayleigh number. In contrast the opposite behaviour was observed for Bingham fluids for large values of the Bingham number. The relative strengths of buoyancy and viscous forces and the effects of Prandtl number on thermal boundary layer thickness are shown to be responsible for this non-monotonic Prandtl number dependence of the mean Nusselt number $\overline{Nu}$ in Bingham fluids. Moreover, a monotonic behaviour is observed when an "effective" viscosity is used to define an effective Grashof number.

Finally, guided by a scaling analysis, simulation results are used to propose new correlations for $\overline{Nu}$ for both Newtonian and Bingham fluids. These correlations are shown to satisfactorily capture the variation of $\overline{Nu}$ with Ra, Pr and Bn for all the cases considered in this study.

It is important to note that in the present study the temperature dependences of yield stress and plastic viscosity have been neglected as a first step to aid the fundamental understanding of natural convection in Bingham fluids in square enclosures with differentially heated side walls. Although the inclusion of temperature-dependent thermo-physical properties are not expected to change the qualitative behaviour observed in the present study, the inclusion of temperature dependence of plastic viscosity μ and yield stress τ_y is probably necessary for quantitative predictions since μ especially decreases with increasing temperature [20]. As a result of this reduction, the value of the Bingham at which $\overline{Nu}$ approaches to unity (i.e. Bn_{max}) is likely to increase with increasing hot wall temperature T_H when the cold wall temperature T_C is held constant. Thus future investigation on the same configuration with temperature-dependent thermo-physical properties (e.g. τ_y and particularly μ) of Bingham fluids will be necessary for deeper understanding and more accurate quantitative predictions.

Acknowledgements

The visit of OT to Liverpool was funded by the European Union's Erasmus Lifelong Learning Programme and is hereby gratefully acknowledged.

References

[1] G. de Vahl Davis, Natural convection of air in a square cavity: a bench mark numerical solution, Int. J. Numer. Methods Fluids 3 (1983) 249–264.
[2] A.F. Emery, J.W. Lee, The effects of property variations on natural convection in a square cavity, J. Heat Transfer 121 (1999) 57–62.
[3] O. Aydın, A. Ünal, T. Ayhan, Natural convection in rectangular enclosures heated from one side and cooled from above, Int. J. Heat Mass Transfer 42 (1999) 2345–2355.
[4] S. Ostrach, Natural convection in enclosure, J. Heat Transfer 110 (1988) 1175–1190.
[5] A. Bejan, Convection Heat Transfer, John Wiley Sons Inc., New York, 1984.
[6] H. Ozoe, S.W. Churchill, Hydrodynamic stability and natural convection in Ostwald-De Waele and Ellis fluids: the development of a numerical solution, AIChE J. 18 (1972) 1196–1207.
[7] M. Lamsaadi, M. Naïmi, M. Hasnaoui, Natural convection of non-Newtonian power law fluids in a shallow horizontal rectangular cavity uniformly heated from below, Heat Mass Transfer 41 (2005) 239–249.
[8] J. Zhang, D. Vola, I.A. Frigaard, Yield stress effects on Rayleigh–Bénard convection, J. Fluid Mech. 566 (2006) 389–419.
[9] N.J. Balmforth, A.C. Rust, Weakly nonlinear viscoplastic convection, J. Non-Newtonian Fluid Mech. 158 (2009) 36–45.
[10] A. Vikhansky, Thermal convection of a viscoplastic liquid with high Rayleigh and Bingham numbers, Phys. Fluids 21 (2009) 103103.
[11] H.M. Park, D.H. Ryu, Rayleigh–Bénard convection of viscoelastic fluids in finite domains, J. Non-Newtonian Fluid Mech. 98 (2001) 169–184.
[12] M. Lamsaadi, M. Naïmi, M. Hasnaoui, M. Mamou, Natural convection in a vertical rectangular cavity filled with a non-Newtonian power law fluid and subjected to a horizontal temperature gradient, Numer. Heat Trans. A 49 (2006) 969–990.
[13] M. Lamsaadi, M. Naïmi, M. Hasnaoui, Natural convection heat transfer in shallow horizontal rectangular enclosures uniformly heated from the side and filled with non-Newtonian power law fluids, Energy Convers. Manage. 47 (2006) 2535–2551.
[14] W.L. Barth, G.F. Carey, On a natural-convection benchmark problem in non-Newtonian fluids, Numer. Heat Transfer B 50 (2006) 193–216.
[15] W.H. Leung, K.G.T. Hollands, A.P. Brunger, On a physically-realizable benchmark problem in internal natural convection, Int. J. Heat Mass Transfer 41 (1998) 3817–3828.
[16] D. Vola, L. Boscardin, J.C. Latché, Laminar unsteady flows of Bingham fluids: a numerical strategy and some benchmark results, J. Comput. Phys. 187 (2003) 441–456.
[17] H.A. Barnes, The yield stress—a review or 'pialphanutaualpha rhoepsiloniota'—everything flows? J. Non-Newtonian Fluid Mech. 81 (1999) 133–178.
[18] E. Mitsoulis, Flows of viscoplastic materials: models and computations, in: D.M. Binding, N.E. Hudson, R. Keunings (Eds.), Rheology Reviews, 2007, pp. 135–178.
[19] E.J. O'Donovan, R.I. Tanner, Numerical study of the Bingham squeeze film problem, J. Non-Newtonian Fluid Mech. 15 (1984) 75–83.
[20] J. Peixinho, C. Desaubry, M. Lebouche, Heat transfer of a non-Newtonian fluid (Carbopol aqueous solution) in transitional pipe flow, Int. J. Heat Mass Transfer 51 (2008) 198–209.
[21] R.J. Poole, B.S. Ridley, Development length requirements for fully-developed laminar pipe flow of inelastic non-Newtonian liquids, ASME J. Fluids Eng. 129 (2007) 1281–1287.
[22] H. Fellouah, C. Castelain, A. Quld El Moctar, H. Peerhossaini, A numerical study of dean instability in non-Newtonian fluids, ASME J. Fluids Eng. 128 (2006) 34–41.
[23] R.J. Poole, R.P. Chhabra, Development length requirements for fully-developed laminar pipe flow of yield stress fluids, ASME J. Fluids Eng. 132 (3) (2010) 034501.
[24] S.V. Patankar, Numerical Heat Transfer and Fluid Flow, Hemisphere, Washington, DC, 1980.
[25] P.J. Roache, Quantification of uncertainty in computational fluid dynamics, Annu. Rev. Fluid Mech. 29 (1997) 123–160.
[26] J. Cadafalch, C.D. Perez-Segarra, R. Cònsul, A. Oliva, Verification of finite volume computations on steady-state fluid flow and heat transfer, ASME J. Fluids Eng. 124 (2002) 11–21.
[27] C. Ismail, O. Karatekin, Numerical experiments on application of Richardson extrapolation with nonuniform grids, ASME J. Fluids Eng. 119 (1997) 584–590.
[28] B.M. Berkovsky, V.K. Polevikov, Numerical study of problems on high-intensive free convection, in: D.B. Spalding, H. Afgan (Eds.), Heat Transfer and Turbulent Buoyant Convection, Hemisphere, Washington, DC, 1977, pp. 443–455.
[29] E. Mitsoulis, T. Zisis, Flow of Bingham plastics in a lid-driven square cavity, J. Non-Newtonian Fluid Mech. 101 (2001) 173–180.
[30] W. Shyy, M.H. Chen, Effect of Prandtl number on buoyancy-induced transport processes with and without solidification, Int. J. Heat Mass Transfer 33 (1990) 2565–2578.